

## On Geoid Heights Derived From Geos 3 Altimeter Data Along the Hawaiian-Emperor Seamount Chain

A. B. WATTS

*Lamont-Doherty Geological Observatory and Department of Geological Sciences  
Columbia University, Palisades, New York 10964*

Geoid heights derived from the Geos 3 satellite altimeter show relatively short wavelength ( $\lambda \gtrsim 280$  km) geoid highs of 5–12 m over the crest of the Hawaiian-Emperor seamount chain and geoid lows of 1–3 m over flanking regions. These geoid undulations can be generally explained by a simple model in which the load of the seamount chain is supported by a strong, rigid lithospheric plate. The best fitting estimates of the effective elastic thickness of the plate based on data over the Hawaiian Ridge are in the range 25–37.5 km. The elastic thickness cannot be reliably determined from altimeter data over the Emperor Seamounts, although it is probable that it is significantly lower than that obtained for the Hawaiian Ridge. These estimates of the differences in elastic thickness along the seamount chain are in general agreement with previous studies along the chain and provide useful new constraints on the long-term ( $>10^6$  years) mechanical properties of the oceanic lithosphere.

### INTRODUCTION

Studies of the earth's gravity field have long been recognized as one of the principal means of deducing geological structure in oceanic regions. Since the development of plate tectonics two approaches to the interpretation of marine gravity anomalies have proven useful. The first approach, based on pioneering studies of *Vening Meinesz* [1941] and *Gunn* [1943], uses relatively short wavelength ( $\lambda \sim 250$  km) gravity anomalies over surface loads of long duration ( $>10^6$  years) to determine information on the long-term mechanical properties of the lithospheric plates [e.g., *Watts and Cochran*, 1974]. The second approach uses the correlation between relatively long wavelength ( $\lambda \sim 2500$  km) gravity anomalies and bathymetry, which exists in some parts of the oceans [*Sclater et al.*, 1975; *Watts*, 1976], to deduce information on the forces acting on the plates and which may ultimately drive them [e.g., *McKenzie*, 1977].

The only global solutions of the earth's gravity field, however, have come from combination solutions of terrestrial and satellite gravity data. One of the most recent earth models, GEM 8 [*Wagner et al.*, 1976], resolves information on the long-wavelength ( $\lambda > 1600$  km) gravity field. Information on the short-wavelength ( $\lambda < 1600$  km) field is based largely on surface measurements, and these are generally sparse over the southern oceans.

There is therefore much geophysical interest in the recent NASA Skylab S-193 [*Leitao and McGoogan*, 1975; *McGoogan et al.*, 1975] and Geos 3 [*Leitao et al.*, 1975] missions, which attempt to determine the gravity field over the oceans with radar altimeters on orbiting satellites. Satellite altimeters measure directly the distance between the satellite and the ocean surface. If the orbit of the satellite is accurately known, the height of the ocean surface relative to an earth reference ellipsoid can be estimated. Since disturbing oceanographic effects are generally less than 1 m, this height closely approximates the shape of the marine geoid.

The Geos 3 satellite [*Leitao et al.*, 1975], which was launched in April 1975, currently provides the best means to estimate geoid heights in oceanic regions. The radar altimeter on this satellite operates by transmitting a pulse downward and receiving the reflection from the sea surface. The in-

strument is operated either in an intensive or in a global mode [*Leitao et al.*, 1975]. The sea-surface 'footprint' of the instrument is about 4 km (intensive mode) or 14 km (global mode).

A number of ground truth studies have now been carried out to assess the performance of the satellite altimeter. *Chapman and Talwani* [1979] have compared geoid heights derived from Geos 3 altimeter data with  $1^\circ \times 1^\circ$  gravimetric geoids in the Atlantic, Indian, and Pacific oceans. They conclude that although systematic differences in the geoids occur, the altimeter geoid has much better resolution than the  $1^\circ \times 1^\circ$  gravimetric geoid particularly over features such as island arcs, deep-sea trenches, and Atlantic-type continental margins. *Marsh et al.* (unpublished manuscript, 1977) have minimized the differences in the altimetric geoid at more than 19,000 track intersections over the western North Atlantic, attributing the differences mainly to orbital uncertainties. The resulting altimetric geoid agreed closely with a detailed  $5' \times 5'$  gravimetric geoid and did not differ by more than 1 m even over relatively short wavelength features such as Bermuda and the Blake escarpment.

The geoid heights derived from satellite altimeter data include both geodetic and oceanographic effects. Thus in order to separate oceanographic effects it is necessary first to remove the geodetic effects. One approach is to compare the geoid heights derived from altimeter data with a detailed gravimetric geoid in the region. The main difficulty with this is that with the possible exception of the western North Atlantic sufficiently accurate gravimetric geoids do not now exist over the oceans.

A useful approach to the problem, however, is to establish whether geological features on the ocean floor are associated with geoid anomalies and then to establish simple models to interpret them. A number of studies have now been carried out which show there is a significant contribution of bathymetry to marine gravity anomalies at least between wavelengths of about 20 and 400 km [*Talwani et al.*, 1972; *McKenzie and Bowin*, 1976; *Watts*, 1978]. The contribution is reduced at shorter wavelengths ( $\lambda \lesssim 20$  km) because of instrument noise and at larger wavelengths ( $\lambda \gtrsim 400$  km) because of the effects of isostatic compensation.

The main problem in evaluating the contribution to the marine geoid of geological features on the ocean floor is that

the bathymetry beneath a satellite track is poorly known. Although existing bathymetry maps generally define the areal extent of features on the ocean floor, they are not, in general, sufficiently accurate to construct bathymetry profiles along a subsatellite track.

The purpose of this paper is to examine the geoid heights derived from preliminary Geos 3 satellite radar altimeter data over the Hawaiian-Emperor seamount chain. Previous studies [Walcott, 1970; Watts and Cochran, 1974; Watts, 1978], based on gravity and bathymetry data, have provided useful information on the state of isostasy along the chain. There are two main objectives to this study: first, to evaluate the contribution of the topography of the seamount chain and its compensation to the marine geoid and, second, to evaluate whether geoid heights derived from Geos 3 satellite altimeter data can be used to provide information on isostasy at geological features such as the Hawaiian-Emperor seamount chain which formed as relatively young loads on the oceanic lithosphere.

#### GEOS 3 ALTIMETER DATA

The geoid heights used in this study were derived from altimeter data obtained by the Geos 3 satellite between May and October 1975 over the Central Pacific Ocean. The data were acquired while the instrument was operated in the intensive mode and have been smoothed over time frames of either 2.2 or 3.2 s (Table 1). Geoid heights have been corrected for the M-2 ocean tide using the model of Hendershott [1973] and have been referred to an ellipsoid with flattening 1/298.255 and semimajor axis 6378.145 km. The Geos 3 data are presented either as profiles along individual satellite tracks (Figure 1) or as profiles projected normal to the local bathymetric trend of the Hawaiian-Emperor seamount chain (Figures 2, 3, 6, and 7).

The main features of these profiles are a relatively short wavelength ( $\lambda \sim 280$  km) geoid high over the crest of the Hawaiian-Emperor seamount chain and a geoid low over flanking regions (Figures 1 and 2). The geoid high reaches a maximum of about 12 m on profile G2676 (Figure 1) near Molokai Island, and the geoid low reaches a maximum of about 6 m on profile G4949 (Figure 1) near Suiko Seamount.

TABLE 1. Summary of Altimeter Data Along the Hawaiian-Emperor Seamount Chain

Lamont I.D.	Orbit Number	Orbital Accuracy*	Day	Figures
G4929	2605	J	285	1
G4841	2150	D	252	1, 3
G4788	1894	D	234	1, 3, 4
G4806	1965	D	239	1, 3
G4949	2690	J	291	1, 3, 4
G4811	1979	J	240	1, 3
G1695	1993	J	241	1, 3
G4481	2263	J	260	1
G4477	2206	J	256	1
G4478	2220	J	257	1
G4458	1438	J	202	1, 3
G4493	2433	J	272	1
G0878	599	J	142	1, 3, 4, 8
G4488	2390	J	269	1
G1113	2859	J	302	1, 3
G0644	2674	J	289	1, 2, 3, 4, 8
G0843	1821	J	229	1, 3, 8
G2676	2361	J	266	1, 3, 4, 7, 8

All data were obtained in 1975 while the Geos 3 transmitter was operated in the intensive mode.

\*D represents 3–10 m rms; J represents 3 m rms.

The geoid lows are particularly prominent on profiles of the Emperor Seamounts (Figure 2).

Figures 1 and 2 show that the relatively short wavelength geoid undulations are superimposed on a relatively long wavelength ( $\lambda \gtrsim 2600$  km) geoid high of about 5–7 m over the southeastern end of the Hawaiian Ridge (east of longitude 177°W). This high appears to be associated with the broad topographic rise or swell around the southeastern end of the Hawaiian Ridge first described by Betz and Hess [1942].

The geoid undulations over the Hawaiian Ridge and Hawaiian swell are superimposed on a longer-wavelength geoid undulation which increases from northeast to southwest across the map area (Figure 1). This increase is up to about 30–40 m and corresponds to the northern gradient of the geoid high centered over the Fiji Plateau. This high is clearly seen in previous global earth models such as the detailed GEM 6 field [Marsh and Vincent, 1974] which do not incorporate altimeter data.

Figure 3 illustrates the relationship between geoid heights and bathymetry for profile G0644 of the Hawaiian Ridge and swell near Nihoa Island (Figure 1). The geoid heights in this figure are observed geoid heights derived from Geos 3 altimeter data with the detailed GEM 6 geoid [Marsh and Vincent, 1974] subtracted from it. The purpose of removing this field is that it describes the longer wavelength geoid undulation associated with the Fiji Plateau which does not appear to be associated with any bathymetric features in the Central Pacific Ocean. The bathymetry profile in the figure was constructed from available bathymetry maps of the Central Pacific Ocean [Chase et al., 1970]. The heavy dots on the profile represent the position of the intersection of a bathymetric contour with the subsatellite track. It is noted that although these maps are the most accurate now available, substantial errors may arise in profiles constructed from the maps because of the lack of surface ship bathymetry measurements along a subsatellite track. The main feature of the profile (Figure 3), however, is a relatively short wavelength ( $\lambda \gtrsim 280$  km) geoid high of about 7 m over the Hawaiian Ridge which is superimposed on a long-wavelength ( $\lambda \gtrsim 2400$  km) geoid high of about 5 m over the swell. The Musician Seamounts, which are located on the northern flanks of the swell and consist of a number of east-west-trending ridges, do not appear to be associated with a geoid high. The Line Islands, which are located southwest of the swell and form part of a northwest-southeast-trending ridge (Figure 1), appear to be associated with a small-amplitude geoid high of about 2 m.

A number of previous studies of gravity and bathymetry data along the Hawaiian-Emperor seamount chain have been carried out [Vening Meinesz, 1941; Walcott, 1970; Watts and Cochran, 1974; Watts, 1978]. These studies have shown that the relatively short wavelength ( $\lambda \gtrsim 250$  km) gravity anomalies along the chain can be largely explained by the gravity effect of the topography and its compensation. The most satisfactory model of compensation which best explains the relationship between gravity and bathymetry along the chain is for a plate (or flexure) model in which the load of the seamount chain is supported by the lithosphere for long periods of geological time. Thus the relatively short wavelength geoid undulations observed along the chain (Figures 1 and 2) should, in a similar way, provide information on the mechanism of isostasy along the chain.

The studies by Watts and Cochran [1974] and Watts [1976] have also established that there is a relatively long wavelength ( $\lambda \gtrsim 2400$  km) gravity anomaly high over the Hawaiian swell.



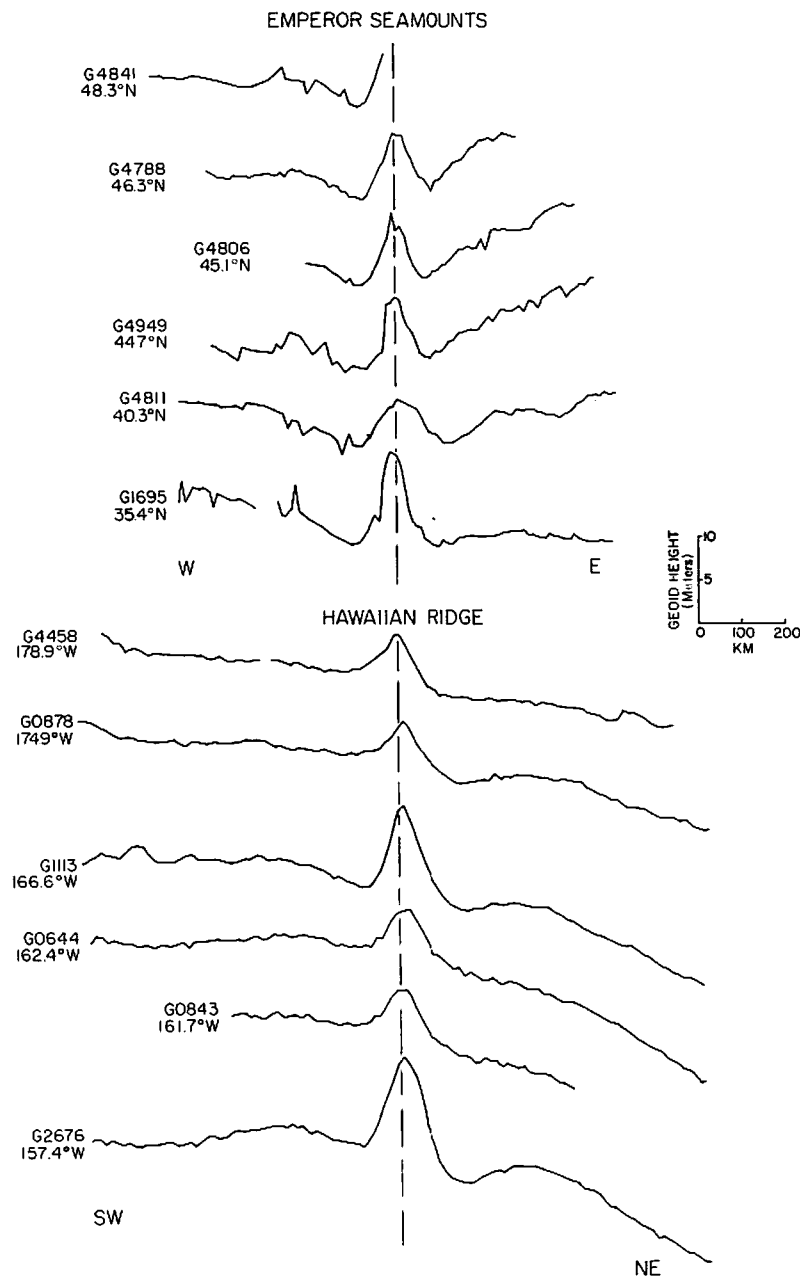


Fig. 2. Selected Geos 3 profiles of the Emperor Seamounts and Hawaiian Ridge. Each profile is located in Figure 1 and has been projected normal to the local trend of the seamount chain. The geoid lows are most prominent on profiles of the Emperor Seamounts. The latitude (Emperor Seamounts) and longitude (Hawaiian Ridge) indicate the approximate position of the intersection of each profile with the crest of the seamount chain.

distributions it is convenient to divide the body into a number of finite horizontal plane lamina. The gravity anomaly  $\Delta g$  due to a lamina of thickness  $\Delta z$  [Talwani, 1973] is

$$\Delta g = G\rho \Delta z \int \left[ 1 - \frac{z}{(z^2 + r^2)^{1/2}} \right] d\psi \quad (1)$$

and the corresponding potential  $V$  is

$$V = G\rho \Delta z \int [(z^2 + r^2)^{1/2} - z] d\psi \quad (2)$$

where  $G$  is the gravitation constant,  $\rho$  is the density,  $z$  is the depth (positive downward),  $d\psi$  is the ordinary angle between a point on the boundary of the lamina and the projection of the observation point on the  $z$  plane,  $r$  is the distance in the plane

of the lamina between a point on the boundary of the lamina and the projection of the observation point, and the line integral is evaluated around the boundary of the lamina. For a polygonal boundary the line integral can be calculated exactly. Each body is described by a series of contours at various depths, and the total potential is found by numerical integration over  $z$ . The total potential  $T$  can be converted to a geoid height  $N$  by Brun's formula

$$N = T/g \quad (3)$$

where  $g$  is the average gravity on the earth's surface.

The crustal model in Figure 4 is based on the flexure model for the compensation of geological features on the earth's surface. This model has been widely used [Vening Meinesz,

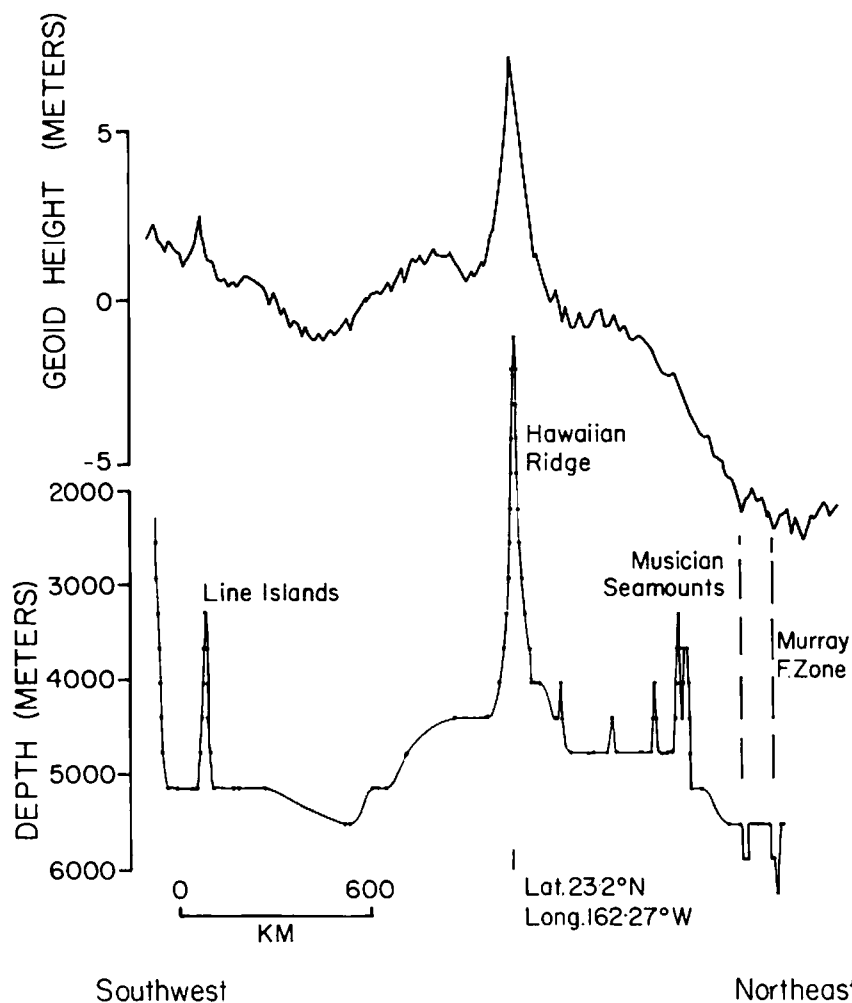


Fig. 3. Geos 3 profile G0644 (Figure 1) and bathymetry profile of the Central Pacific Ocean between the Line Islands and the Murray Fracture Zone. The observed Geos 3 profile has had the GEM 6 earth model subtracted from it [Marsh and Vincent, 1974]. The bathymetry profile has been constructed using the contour maps of Chase et al. [1970]. Heavy dots indicate the location of individual contours. The Hawaiian Ridge and Line Islands are associated with geoid highs of 6 and 2 m, respectively. The Musician Seamounts and the Murray Fracture Zone, however, are not associated with prominent geoid highs or lows.

1941; Walcott, 1970; Watts and Cochran, 1974] to study lithospheric flexure caused by surface loads such as seamount chains. In this model the seamount chain represents a load on a thin elastic plate which overlies a weak fluid substratum. The most useful parameter in flexure models is the flexural rigidity  $D$ , which is determined by the elastic thickness of the plate. Figure 4 shows computed geoid profiles for a theoretical seamount load (the size and average density of the load have been chosen to closely represent that for the Hawaiian-Emperor seamount chain) and for assumed values of the flexural rigidity of  $1 \times 10^{29}$ ,  $1 \times 10^{30}$ , and  $1 \times 10^{31}$  dyn cm. These values were chosen since they represent the range of previous estimates of the flexural rigidity of the oceanic lithosphere based on gravity and bathymetry studies.

Figure 4 shows there are significant differences in the computed geoid for different values of the flexural rigidity. The geoid high over the seamount chain for a flexural rigidity of  $1 \times 10^{29}$  dyn cm is 6 m but for a rigidity of  $1 \times 10^{31}$  dyn cm is 16 m. Thus if there are significant differences in the flexural rigidity along the seamount chain, it should be possible to use Geos 3 altimeter data to resolve them.

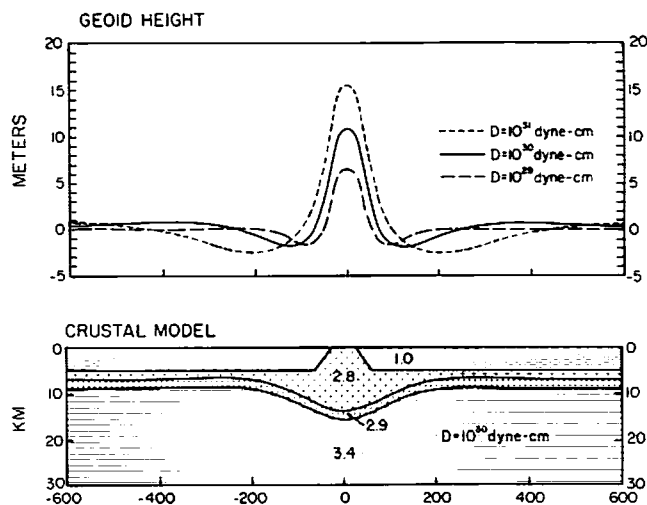


Fig. 4. Theoretical geoid profiles over a 60-km-wide seamount chain for different assumed values of the effective flexural rigidity of the oceanic lithosphere,  $D$ .

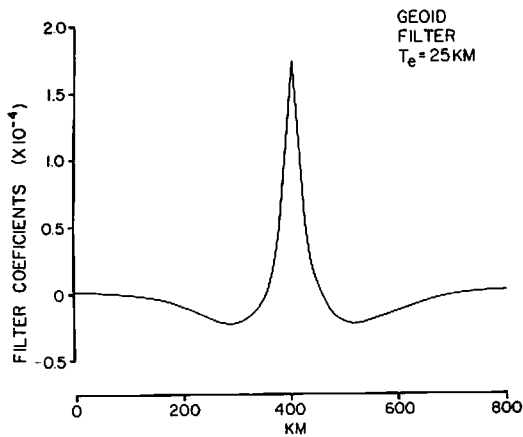


Fig. 5. Theoretical geoid filter corresponding to an effective flexural rigidity of the oceanic lithosphere of  $1.5 \times 10^{30}$  dyn cm, corresponding to an elastic thickness of 25 km. The filter was obtained by inverse Fourier transforming the admittance  $Z'(k)$  associated with the flexure (or plate) model of isostasy. The filter can be considered as an impulse response function representing the geoid effect of a line load on the earth's surface.

The procedure used by *Watts and Cochran* [1974] was to compute the flexure of the lithosphere due to the seamount load and then compute the combined gravity effect of the load and its compensation. The best fitting flexural rigidity at the seamount was then selected as that value which minimized the

sums of the squares of the residuals between observed and calculated gravity anomalies.

A more convenient way to compute the gravity or geoid effect due to a surface load and its compensation, however, is to use linear transfer function techniques [*Lewis and Dorman*, 1970; *McKenzie and Bowin*, 1976]. Theoretical filters can be constructed using these techniques which represent the gravity or geoid effect of a unit load on the surface of the plate. Thus by convolution of these filters with observed elevation or bathymetry data gravity profiles can easily be computed for different values of flexural rigidity and compared with observed profiles.

*McKenzie and Bowin* [1976] and *Watts* [1978] have given expressions for the transfer function (or admittance  $Z(k)$ ) which describe the relationship between gravity and bathymetry as a function of wave number for the flexure model. The expressions given in these two studies differ only in the oceanic crustal structure which is assumed. The corresponding admittance  $Z'(k)$  which describes the relationship between geoid and bathymetry as a function of wave number can then be obtained [e.g., *Chapman*, 1979] by

$$Z'(k) = Z(k)/gk \quad (4)$$

where  $k = 2\pi/\lambda$ . The corresponding filter can then be obtained by applying the inverse Fourier transform to  $Z'(k)$ .

Figure 5 shows a theoretical filter for an assumed flexural rigidity of the plate of  $1.5 \times 10^{30}$  dyn cm, which corresponds to an elastic plate thickness of 25 km (assuming Young's modu-

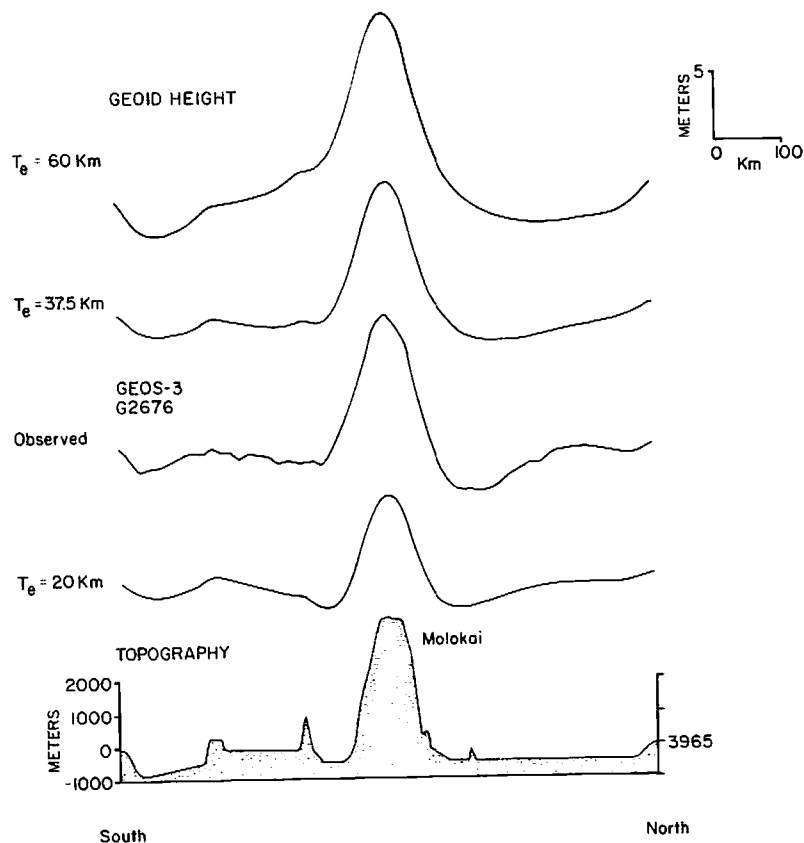


Fig. 6. Computed geoid heights compared to Geos 3 profile G2676 (Figure 1) of the Hawaiian Ridge near Oahu. The computed profiles were obtained by convolving theoretical geoid filters with the bathymetry profile for different assumed values of the elastic thickness. Note that the amplitude of the computed geoid profile for an elastic thickness of 20 km is smaller than the observed and that the amplitude for an elastic thickness of 60 km is larger than the observed. The best fit, in a least squares sense, is for an elastic thickness of 37.5 km.

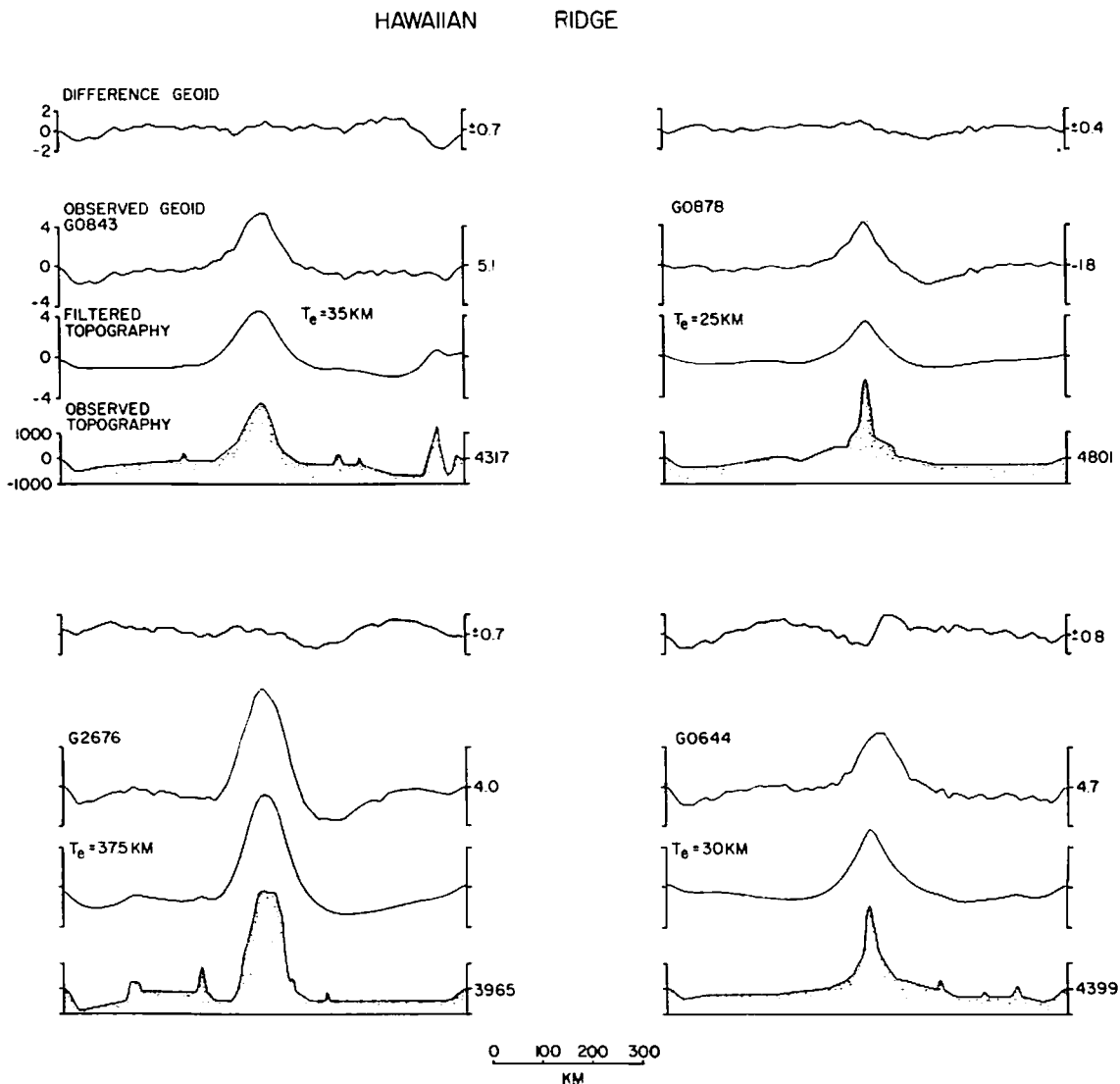


Fig. 7. Comparison of selected Geos 3 profiles of the Hawaiian Ridge (Figure 1) to theoretical profiles based on the flexure model of isostasy. The filtered topography profiles were obtained by convolving theoretical filters with the observed topography. The difference geoid is the difference between the observed and calculated geoid heights. The units for each of the profiles are in meters. The variance associated with the best fitting value is shown to the right of each difference geoid profile and does not exceed  $\pm 0.8$  m on any of the profiles.

lus  $E = 10^{12}$  dyn  $\text{cm}^{-2}$ ). The filter is 800 km long and shows a broad peak flanked by prominent side lobes.

The theoretical filter in Figure 5 was convolved with the theoretical seamount load in Figure 4 and the computed geoid compared with the geoid based on the line-integral method. The two geoids agreed closely. The only differences were over the crest of the seamount chain and at the ends of the profile. These differences did not exceed 1 m and can be largely attributed to the method used to remove the mean from the bathymetry profiles and to tapering their ends.

#### RESULTS

The geoid heights derived from Geos 3 altimeter data are compared with computed profiles based on the flexure model on 4 selected profiles of the Hawaiian Ridge in Figures 6 and 7. The computation procedure is similar to that described by Watts [1978]. Theoretical filters were constructed for different values of the elastic thickness of the plate ( $T_e$ , Figures 6 and 7). The mean and trend were then removed from each bathymetry profile and the ends of each profile tapered to zero. The main

difference is in the method of filtering. In this study, computed geoid profiles were obtained by the convolution of the theoretical filters with the observed bathymetry. The ends of each bathymetry profile were padded with zeros to prevent aliasing at the ends of the profiles.

Figure 6 compares profile G2676 (Figure 1) of the southeastern end of the Hawaiian Ridge with computed profiles based on different assumed values of the elastic thickness of the oceanic lithosphere. This figure shows that the computed geoid height for a plate thickness  $T_e = 20$  km is too small (7.5 m) in amplitude compared with the observed geoid height (12 m) and that the computed height for  $T_e = 60$  km is too large (15 m). The most satisfactory fit to both the amplitude and the wavelength of the observed geoid height is for a plate thickness of  $T_e = 37.5$  km (Figure 6).

The comparison in Figure 6 suggests that it should be possible to estimate reliably the elastic thickness ( $T_e$ ) of the oceanic lithosphere from Geos 3 altimeter data. Figure 7 shows the 'best fit' estimate of the elastic thickness for three other profiles of the Hawaiian Ridge. The best fit elastic thickness

was estimated as that value which minimized the difference between observed and computed profiles. The best fitting estimates of the elastic thickness range from 25 to 37.5 km and the rms difference does not exceed  $\pm 0.8$  m on any of the profiles.

Figure 7 shows that a significant part of the altimetric geoid can be explained by the geoid effect of the topography of the seamount chain and its compensation. The computed profiles generally explain both the amplitude and the wavelength of the observed profiles. The difference geoids in this figure therefore represent the contribution to the altimetric geoid which cannot be attributed to the geoid effect of the topography of the seamount chain and its compensation. Thus the geodetic (or tectonic) contribution to the altimetric geoid appears to have been isolated from other contributions. It is unlikely, however, that the difference geoids represent the contribution of oceanographic effects to the altimetric geoid. Significant differences between observed and computed geoids could arise owing to uncertainties in bathymetry (for example, profile G0644) or to density variations in the oceanic crust which have not been taken into account in the simple model of flexure.

The range of best fitting estimates of the elastic thickness can also be determined by computing the admittance from the observed geoid and bathymetry data. The observed admittance contains information on the model of isostasy along the seamount chain. The main problem is determining smooth estimates of the admittance from the observed data. *McKenzie and Bowin* [1976] obtained smooth estimates by dividing their long gravity and bathymetry profiles into a number of shorter subprofiles. They then averaged the spectra for each subprofile for a particular wavenumber. *Watts* [1978] used a method more suitable for the study of a single geological feature. In this method a number of similar length gravity and bathymetry profiles over the same geological feature are used, each of which constitutes an independent estimate of the relationship between gravity and bathymetry. The spectra are then averaged for each profile for a particular wave number.

The geoid and bathymetry profiles in Figure 7 were used to generate admittance values for the Hawaiian ridge. The basic computational steps were similar to those used by *Watts* [1978] for gravity and bathymetry data. The observed geoid and bathymetry profiles were used to estimate the cross spectrum and power spectrum and to construct an average over the four profiles (Figure 7). The admittance was obtained by dividing the cross spectrum of the geoid and bathymetry by the power spectrum of the bathymetry. The smoothed spectra were also used [e.g., *McKenzie and Bowin*, 1976] to compute the coherence and the phase of the admittance.

The results of the computations are summarized in Table 2. The relative smoothness of the admittance values for  $0.0078 <$

TABLE 2. Spectral Estimates for Geos 3 Altimeter Profiles of the Hawaiian Ridge

Wave Number $k, \text{ km}^{-1}$	Coherence $\gamma^2$	Phase $\phi$	Sample Admittance, $\text{m/km}$	Noise Parameter $\sigma$
0.0078	0.929	-3.1	2.4	0.097
0.0156	0.910	-6.3	3.0	0.111
0.0235	0.915	-2.1	3.4	0.107
0.0313	0.972	8.4	2.2	0.060
0.0391	0.747	3.3	1.5	0.206
0.0469	0.780	7.1	1.2	0.187
0.0548	0.198	33.9	0.5	0.711
0.0626	0.392	6.2	1.0	0.440

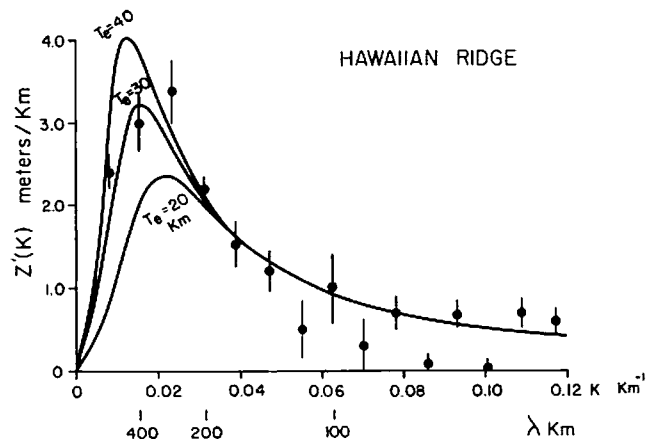


Fig. 8. Admittance ( $Z'(k)$ ) values generated from observed Geos 3 and bathymetry profiles in Figure 7. The standard error on each estimate is computed from the coherence (Table 2) assuming a normal probability distribution for the ratio of true/sample admittance [*Munk and Cartwright*, 1966]. The solid lines represent theoretical models based on the plate model for an assumed mean water depth of 4.335 km, density of topography of  $2.80 \text{ g cm}^{-3}$  [*Watts*, 1978], and effective elastic thickness values of  $T_e = 20, 30,$  and  $40$  km.

$k < 0.0469$  is evidence that a similar signal was present in each profile and that the smoothing procedure satisfactorily reduces the noise. The phase of the admittance is approximately zero for these wave numbers, indicating that the admittance is real. The coherence is high ( $> 0.7$ ) for  $k \gtrsim 0.0469$ , suggesting that for wavelengths longer than about 130 km a significant part of the energy in the observed geoid is caused by the bathymetry.

The observed admittance values (Table 2) are compared with calculated admittance curves based on the flexure model in Figure 8. The computed admittance curves increase gently because short-wavelength topography is uncompensated and then decrease sharply because of the effects of isostatic compensation. The 'critical' wavelength at which isostasy becomes important depends on the value of the elastic thickness assumed for the plate. Although there is some scatter, Figure 8 shows that the best fit to the observed admittance values is for an elastic thickness in the range 28–37 km, in general agreement with the estimates obtained in Figure 7. The critical wavelength for geoid data along the Hawaiian Ridge cannot be determined very precisely but appears to be in the range 260–400 km (Figure 8).

#### TECTONIC IMPLICATIONS

Geoid heights derived from Geos 3 satellite altimeter data have therefore been used to estimate the elastic thickness of the oceanic lithosphere along the Hawaiian Ridge. The best fitting values are in the range 25–37.5 km. It is important to note that the elastic thickness determined from the altimeter data is not the actual thickness of the lithosphere. It is the thickness the lithosphere would have if it responded to long-term ( $> 10^6$  years) loads as an elastic plate overlying a weak fluid. The elastic thickness is much less than the seismic or thermal thickness of the lithosphere. Apparently, in response to long-term loads only the upper part of the plate responds elastically.

*Watts* [1978] has suggested, on the basis of gravity and bathymetry studies in the Pacific Ocean, that the elastic thickness acquired at long-term loads depends on the temperature gradient of the lithosphere at the time it is loaded. Surface loads, such as ridge crest topography, which form on relatively young oceanic lithosphere are associated with small values of

the elastic thickness, while surface loads, such as the Hawaiian Ridge, which form on relatively old oceanic lithosphere are associated with large values of the elastic thickness. This increase can be reasonably well fit by a simple model in which the elastic thickness represents the depth to the 450°C oceanic isotherm (Figure 9).

The results from the Geos 3 altimeter data used in this study are shown as a solid triangle in Figure 9. The age of the lithosphere at the time of loading has been estimated from age data along the seamount chain [Clague and Jarrard, 1973] and from inferred age of the sea floor based on magnetic lineations. Figure 9 shows that the Geos 3 altimeter results are in good agreement with those from previous studies based on gravity and bathymetry data along the chain.

An important test of the hypothesis that the elastic thickness depends on the age of the lithosphere at the time of loading is gravity or geoid data over the Emperor Seamounts. The Emperor Seamounts between about latitudes 40°N and 49°N are 52–58 m.y. old and are underlain by oceanic crust which is about 80 m.y. old [Clague and Jarrard, 1973; Hilde, 1973]. Thus the age of the oceanic lithosphere at the time of loading is about 28–22 m.y. Figure 9 shows that the Emperor Seamounts north of 40°N should be associated with smaller values for the elastic thickness than for the Hawaiian Ridge. Watts [1978] has estimated the elastic thickness for the Emperor Seamounts north of 40°N in the range 10–20 km, but these estimates are based on only three gravity and bathymetry profiles.

Although a number of Geos 3 satellite tracks cross the Emperor Seamounts north of latitude 40°N (Figure 1), it is not possible to use the data to estimate the elastic thickness of the oceanic lithosphere reliably. There are two main problems. First, the satellite tracks intersect the seamount chain at a high angle. Second, the bathymetry in the region of the seamounts is only poorly known.

Figures 1 and 2 show, however, that in comparison with Geos 3 data over the Hawaiian Ridge there is a smaller-amplitude geoid high over the crest of the seamounts and more prominent geoid lows over flanking regions. Simple model calculations (for example, Figure 4) suggest that these profiles would require smaller values of the elastic thickness. Thus Geos 3 data are in qualitative agreement with relatively low values of the elastic thickness associated with the Emperor Seamounts north of 40°N.

The Geos 3 altimeter data cannot therefore be reliably used in support of the suggestion that the lithosphere is capable of supporting large loads on the surface of the plates for periods of geological time of the order of the age of the Emperor Seamounts. The principal evidence for this suggestion is the evidence from gravity and bathymetry that the elastic thickness at the Emperor Seamounts north of 40°N was acquired at the time of loading and that it has not subsequently changed with time (Figure 9).

The range of elastic thickness estimates determined from Geos 3 data over the Hawaiian Ridge do not appear, however, to be able to explain the observed geoid over features flanking the seamount chain such as the Musician Seamounts and Line Islands Ridge (Figures 3 and 7). These features probably require much lower values of the elastic thickness. One possibility is that these features originated at or near a mid-oceanic ridge crest rather than in the interior of a relatively old lithospheric plate.

We have therefore explained a significant part of the altimetric geoid in terms of the topography of the seamount chain and its compensation. This result is important, since this litho-

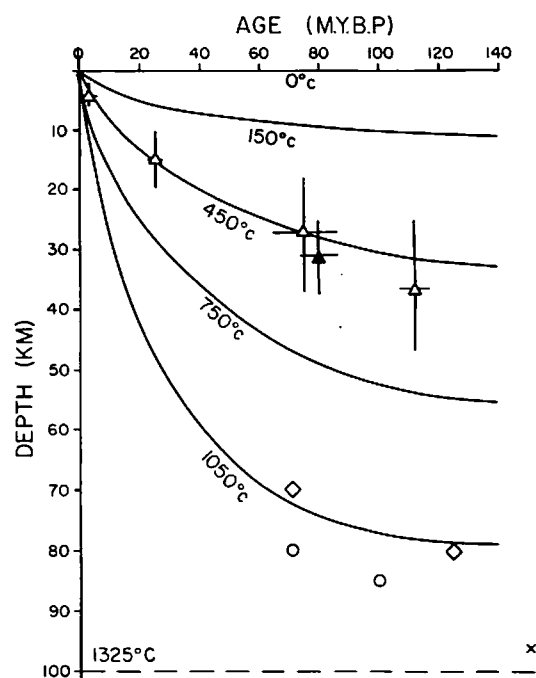


Fig. 9. Comparison of previous estimates of the elastic thickness of the Pacific Ocean lithosphere (open triangles; Watts [1978]) with the estimates obtained in this study (solid triangle). The solid lines are oceanic isotherms based on a simple cooling plate model with assumed initial temperature of 1325°C, heat capacity of  $0.3 \text{ kcal g}^{-1} \text{ }^\circ\text{C}^{-1}$ , and thermal conductivity of  $7.5 \times 10^{-3} \text{ kcal }^\circ\text{C}^{-1} \text{ cm}^{-1} \text{ s}^{-1}$ . The estimates from this study are in good agreement with previous estimates and support the hypothesis that the elastic thickness depends on the age of the oceanic lithosphere at the time of loading.

spheric effect can now be removed from the measured geoid height and residual profiles interpreted in terms of mass distributions either at depth within the lithosphere or beneath it. Of particular interest is the origin of the long-wavelength geoid high over the Hawaiian swell (Figure 3). Future studies which use Geos 3 data over the Pacific Ocean should be able to establish the source of the geoid high and whether or not it is related to deep processes in the earth such as mantle convection.

#### CONCLUSIONS

This analysis of geoid heights derived from available Geos 3 satellite altimeter data along the Hawaiian-Emperor seamount chain allows the following conclusions to be made.

1. The Geos 3 satellite altimeter has successfully recovered short-wavelength ( $\lambda \sim 280 \text{ km}$ ) geoid highs of 5–12 m over the Hawaiian-Emperor seamount chain and geoid lows of 1–3 m over flanking regions.

2. These geoid undulations can be explained by a simple model in which the oceanic lithosphere supports the weight of the seamount chain for long periods of geological time.

3. The best fitting elastic thickness of the oceanic lithosphere based on the altimeter data is in the range 25–37.5 km.

4. The difference between observed and calculated geoid heights based on these thicknesses is small and does not exceed an rms discrepancy of  $\pm 0.8 \text{ m}$  on any of the profiles.

5. The elastic thickness estimates deduced from the Geos 3 altimeter data are in substantial agreement with values based on surface ship gravity and bathymetry observations and provide further support for the hypothesis that the elastic thickness acquired at a surface load depends on the temperature gradient of the lithosphere at the time of loading.

6. The Geos 3 altimeter data are in qualitative agreement with relatively low values of the elastic thickness along the Emperor Seamounts. However, they cannot now be reliably used in support of the hypothesis that the oceanic lithosphere is elastic rather than viscoelastic on long-time scales.

7. The short-wavelength geoid undulations associated with the seamount chain are superimposed on a long-wavelength ( $\lambda \sim 2600$  km) geoid high associated with the Hawaiian swell. This geoid high cannot be explained by the flexure model and is probably caused by mass distributions at depth in the lithosphere or beneath it.

#### APPENDIX: SUMMARY OF PARAMETERS ASSUMED IN MODEL COMPUTATIONS

Thickness of layer 2	1.5 km
Mean thickness of oceanic crust	5 km
Density of mantle	$3.4 \text{ g cm}^{-3}$
Density of layer 3	$2.9 \text{ g cm}^{-3}$
Density of topography	$2.8 \text{ g cm}^{-3}$
Mean water depth	4.3 km
Young's modulus	$10^{12} \text{ dyn cm}^{-2}$

*Acknowledgments.* This work was supported by NASA grant NAS 6-2519 and Office of Naval Research contract N00014-75-C-0210-Scope B. M. Chapman and J. Bodine read an early version of the manuscript and made a number of helpful suggestions. Lamont-Doherty Geological Observatory contribution number 2814.

#### REFERENCES

- Betz, F., and H. H. Hess, The floor of the North Pacific Ocean, *Geogr. Rev.*, **32**, 99-116, 1942.
- Chapman, M., Techniques for interpretation of geoid anomalies, *J. Geophys. Res.*, **84**, this issue, 1979.
- Chapman, M., and M. Talwani, Comparison of gravimetric geoids with Geos 3 altimeter, *J. Geophys. Res.*, **84**, this issue, 1979.
- Chase, T. E., H. W. Menard, and J. Mammerickx, Bathymetry of the North Pacific, charts 5, 6, Scripps Inst. of Oceanogr. and Inst. of Mar. Res., La Jolla, Calif., 1970.
- Clague, D. A., and R. D. Jarrard, Tertiary Pacific plate motion deduced from the Hawaiian-Emperor chain, *Geol. Soc. Amer. Bull.*, **84**, 1135-1154, 1973.
- Detrick, R. S., and S. T. Crough, Island subsidence hot spots and lithospheric thinning, *J. Geophys. Res.*, **83**, 1236-1244, 1978.
- Gunn, R., A quantitative evaluation of the influence of the lithosphere on the anomalies of gravity, *J. Franklin Inst.*, **236**, 373-396, 1943.
- Hendershott, M. C., Tide model ocean tides, *Eos Trans. AGU*, **54**, 76-86, 1973.
- Hilde, T. W. C., Mesozoic sea-floor spreading in the North Pacific, Ph.D. thesis, 84 pp., Univ. of Tokyo, 1973.
- Leitao, C. D., and J. T. McGoogan, Skylab radar altimeter: Short wavelength perturbations detected in ocean surface profiles, *Science*, **186**, 1208-1209, 1975.
- Leitao, C. D., C. L. Purdy, and R. L. Brooks, Wallops Geos-C altimeter preprocessing report, *NASA Tech. Memo. X-69357*, 68 pp., 1975.
- Lewis, B. T. R., and L. M. Dorman, Experimental isostasy, 2, An isostatic model for the U.S.A. derived from gravity and topographic data, *J. Geophys. Res.*, **75**, 3367-3386, 1970.
- Marsh, J. G., and S. Vincent, Global detailed geoid computation and model analysis, *Geophys. Surv. 1*, 481-511, 1974.
- McGoogan, J. T., C. D. Leitao, and W. T. Wells, Summary of Skylab S-193 altimeter altitude results, *NASA Tech. Memo. X-69355*, 323 pp., 1975.
- McKenzie, D. P., Surface deformation, gravity anomalies and convection, *Geophys. J. Roy. Astron. Soc.*, **48**, 211-238, 1977.
- McKenzie, D. P., and C. Bowin, The relationship between bathymetry and gravity in the Atlantic Ocean, *J. Geophys. Res.*, **81**, 1903-1915, 1976.
- Munk, W. H., and D. E. Cartwright, Tidal spectroscopy and prediction, *Phil. Trans. Roy. Soc. London, Ser. A*, 259-533, 1966.
- Slater, J. G., L. A. Lawver, and B. Parsons, Comparison of long-wavelength residual elevation and free-air gravity anomalies in the North Atlantic and possible implications for the thickness of the lithospheric plate, *J. Geophys. Res.*, **80**, 1031-1052, 1975.
- Talwani, M., Computer usage in the computation of gravity anomalies, in *Methods of Computational Physics*, edited by B. Bolt, p. 13, Academic, New York, 1973.
- Talwani, M., H. R. Poppe, and P. D. Rabinowitz, Gravimetrically determined geoid in the western North Atlantic, in *Sea Surface Topography from Space*, vol. 2, *NOAA Tech. Rep. ERL-228-AOML 7-2*, 1-34, NOAA, Boulder, Colo., 1972.
- Vening Meinesz, F. A., Gravity over the Hawaiian Archipelago and over the Madiera area: Conclusions about the earth's crust, *Proc. Kon. Ned. Akad. Wetensia*, **44** pp., 1941.
- Wagner, C. A., F. J. Lerch, J. E. Brownd, and J. A. Richardson, Improvement in the geopotential derived from satellite and surface data (GEM 7 and 8), *NASA/GSFC Doc. X-921-76-20*, Goddard Space Flight Center, Greenbelt, Md., 1976.
- Walcott, R. I., Flexural rigidity, thickness, and viscosity of the lithosphere, *J. Geophys. Res.*, **75**, 3941-3954, 1970.
- Watts, A. B., Gravity and bathymetry in the Central Pacific Ocean, *J. Geophys. Res.*, **81**, 1533-1553, 1976.
- Watts, A. B., An analysis of isostasy in the world's oceans, 1, Hawaiian-Emperor seamount chain, *J. Geophys. Res.*, **83**, 5989-6004, 1978.
- Watts, A. B., and J. R. Cochran, Gravity anomalies and flexure of the lithosphere along the Hawaiian-Emperor seamount chain, *Geophys. J. Roy. Astron. Soc.*, **38**, 119-141, 1974.

(Received May 4, 1978;  
revised July 19, 1978;  
accepted January 8, 1979.)